

# Seismic tests of RC shear walls confined with high-strength rectangular spiral reinforcement

Huajing Zhao, Qingning Li, Can Song\*, Haotian Jiang and Jun Zhao

*Xi'an University of Architecture and Technology, 710055, Xi'an, China*

*(Received November 04, 2016, Revised February 18, 2017, Accepted February 25, 2017)*

**Abstract.** In order to improve the deformation capacity of the high-strength concrete shear wall, five high-strength concrete shear wall specimens confined with high-strength rectangular spiral reinforcement (HRSR) possessing different parameters, were designed in this paper. One specimen was only adopted high-strength rectangular spiral hoops in embedded columns, the rest of the four specimens were used high-strength rectangular spiral hoops in embedded columns, and high-strength spiral horizontal distribution reinforcement were used in the wall body. Pseudo-static test were carried out on high-strength concrete shear wall specimens confined with HRSR, to study the influence of the factors of longitudinal reinforcement ratio, hoop reinforcement form and the spiral stirrups outer the wall on the failure modes, failure mechanism, ductility, hysteresis characteristics, stiffness degradation and energy dissipation capacity of the shear wall. Results showed that using HRSR as hoops and transverse reinforcements could restrain concrete, slow load carrying capacity degeneration, improve the load carrying capacity and ductility of shear walls; under the vertical force, seismic performance of the RC shear wall with high axial compression ratio can be significantly improved through plastic hinge area or the whole body of the shear wall equipped with outer HRSR.

**Keywords:** high-strength rectangular spiral reinforcement; shear walls; pseudo-static test; seismic performance

## 1. Introduction

High-strength concrete has advantages of high strength, high durability and high permeability (Chen 1997). With the rapid development of high-rise buildings and large span buildings, reinforced concrete (RC) structure using high-strength materials has become a kind of inevitable trend. High-strength concrete shear wall structure is adopted in the bottom of high-rise and super high-rise buildings, which can reduce the thickness of the shear wall, increase the utilization rate of the construction area, and has good economic and social benefits. However, the brittleness of high-strength concrete is prominent, the strength gain of high-strength concrete comes at a cost in a loss of ductility with high-strength concrete more brittle than normal strength concrete, that limits the application of high-strength concrete in high-rise buildings in seismic regions (Liang *et al.* 2007).

Through high-strength spiral hoops set in high-strength concrete members, constraints on concrete were strengthened; under the vertical load, core concrete in tri-axial compression, so that the core concrete has higher compressive strength and compressive deformation ability, leading the failure mode of concrete members from brittle to plastic, and improving the shear capacity of RC members. It is much easier to achieve the seismic design principle of "strong shear weak bending" (GB50011-2010

2010).

So far, many scholars have studied the mechanical properties of high-strength concrete member confined with rectangular spiral stirrups, Ten(10) HSC columns confined with high-strength stirrups were experimentally study by Karayannis *et al.* (2005), and it demonstrated that adopting high-strength stirrup confined concrete was an effective method to prevent sharp decline of the stress-strain curve of high-strength concrete. High-strength stirrups could continuously provide great constraining forces after the peak load, obviously improving the ductility performance of confined concrete and thus contributing to seismic performance of structures.

Yin *et al.* (2012) took a series of axial compression tests of 10 confinement designs, including rectilinear configurations and different multi-spiral configurations. The test results showed that the specimens with multi-spiral configurations exhibited higher compressive strengths, energy capacities, and ductility than those with rectilinear confinement designs.

De Corte and Boel (2013) made a test of 24 reinforced concrete beams in a static four-point bending test, the results of which indicated that, within the inclination range used, spirally shaped shear reinforcement was a valid alternative, that could be used in international codes.

The experimental results of these tests revealed that the application of rectangular spiral reinforcements (RSR) in kinds of elements, such as beams, columns, beam-column joints, improved the overall seismic performance of the examined specimens in comparison with the conventionally reinforced sub-assemblages (Jing *et al.* 2016, Eom *et al.* 2014, Tsonos 2004, Karayannis and Sirkelis 2005). Besides,

---

\*Corresponding author, Ph.D.,  
E-mail: [brightscan@126.com](mailto:brightscan@126.com)

Liang *et al.* (2014) proposed that the spirals used in a column were time-saving and cost-effective in both fabrication and construction, because production of the continuous spirals and assembly of the cages can be carried out effectively in the factory. Moreover, Spiral reinforcement can positively and quickly be tied into place, so replacing the individual stirrups by a continuous spiral can reduce the labor cost.

The objective of this paper was to experimentally investigate the seismic behavior of RC shear walls confined with HRSR. Pseudo-static tests were carried out on high-strength concrete shear wall specimens confined with HRSR, to analyze the influence of the factors of longitudinal reinforcement ratio, hoop reinforcement form and outer HRSR on the failure modes, failure mechanism, ductility, hysteresis characteristics, stiffness degradation and energy dissipation capacity of the shear wall. The research in this paper provides experimental database for the seismic performance of high-strength concrete shear walls, especially those under high axial compression ratios. In addition, the published work on the use of rectangular spiral reinforcements as shear reinforcement in RC shear walls with rectangular cross-section is very limited. The work fills a gap which has hitherto existed in RC shear walls.

## 2. Experimental

### 2.1 Specimen design

Five high-strength concrete shear walls confined with HRSR were designed, numbered from HCRCW-01 to HCRCW-05, respectively. The strength grade of the concrete was C50. The cross sectional dimension of the shear wall, height of the wallboard, and shear-span ratio were 100 mm × 1000 mm, 2000 mm, and 2.1, respectively. The testing axial compression ratio of specimens HCRCW-01 to HCRCW-04 were 0.22, and specimen HCRCW-05 was 0.17. A reinforced concrete loading beam was set on the top of the wall in order to apply the reversed horizontal load with a distance between the action spot and the wall top of 100 mm. A rigid grade beam with a dimension of 400 mm × 500 mm × 1800 mm was set on the bottom of the wall and casted together with the shear wall as a whole.

Embedded columns were set within the range of 200 mm on both sides of the wall cross section, and longitudinal bars were densely configured in the embedded column regions on the two sides of the wallboard in order to simulate the stirrup configuration of the embedded columns of shear wall. For the purposes of increasing the confining effect of reinforcement on the concrete, improving the ductility of high-strength concrete shear wall, and enhancing the shear-load carrying capacity of the shear wall, the following three measures were taken on specimens HCRCW-01 to HCRCW-04.

- (1) HRSR with a diameter of 5 mm and a tensile strength of 1120 MPa were adopted in the embedded columns on both sides of the shear wall.
- (2) Horizontal distribution reinforcements in the shear wall were replaced by the HRSR with a diameter

of 5 mm; high-strength reinforcement bars with a diameter of 5 mm were used of common form as the vertically distribution reinforcement bars.

- (3) HRSR were adopted with the piece-confining configuration like a chain (Liang *et al.* 2007). That was, the confining range of spiral reinforcements was divided into multiple independent confining segments, where concrete in each segment was confined separately. HRSR in each independent segment were connected at the joint with vertical steel bars. Horizontal spiral reinforcement bars were mutually nested at locations where vertical reinforcement bars were configured.

In addition, the plastic hinge region and the all of wall body of HCRCW-03 and HCRCW-04 were outer HRSR (setting high-strength rectangular spiral reinforcement outside the concrete protective layer) with a diameter 5mm spacing 60 mm, respectively. In wall corners and main load points were set vertical reinforcements with a diameter 5 mm, and formed steel mesh skeleton with outer HRSR. The embedded columns on both sides of the specimen HCRCW-05 were adopted HRSR with a diameter of 5 mm and a tensile strength of 1120 MPa, the horizontal and vertical distribution reinforcements were adopted ordinary form with diameter 4mm and 8mm of HPB300 grade heat treated steel bar, respectively. HCRCW-05 was a benchmark specimen, compared to the specimen SW11 of literature (Zhang *et al.* 2009). The main differences between the two specimens were the ratio of horizontal distribution reinforcement and vertical distribution reinforcement as well as stirrup form in the embedded columns. A 135° hook segmented was constrained in the confining regions in specimen SW11. However, high-strength rectangular spiral stirrups were adopted in the embedded columns and the constraint of spiral hoops were closed in HCRCW-05.

Specimen dimensions and reinforcement configuration were shown in Fig. 1. Details of specimens were shown in Table1, and the measured material indexes of reinforcements and concrete were shown in Tables 2-3.

### 2.2 Loading equipment and loading mechanism

The experiment was implemented in the Key Lab of Structure Engineering and Earthquake Resistance, Ministry of Education, Xi'an University of Architecture and Technology. The pseudo-static loading equipment was shown in Fig. 2. Horizontal loads were provided by the reciprocating actuator with the loading point at the center of the loading beam on the top of the wall. The pushing load direction of the actuator was specified as the positive direction and the pulling direction as the negative. Vertical loads were applied by a 2000 kN oil jack. In order to remain the action spot of the vertical load always at the top center of the wall and keep it synchronous and same direction with the specimen deformation in the test, a sliding support was assembled on the counter-force beam and a 2000 kN jack was reversely assembled on the sliding support. A rigid beam seat was configured between the vertical jack and the specimens so that uniform compressive stress could be generated on the cross section of the shear wall. A mudsill

was fixed on the rigid pedestal by using ground anchor bolt and compression beam, and the in-plane sliding and out-of-plane displacement of the specimen were confined by applying the anti-skid jack and out-of-plane support. In the test, a vertical load was first applied by the oil jack using the midpoint loading method so that the load was uniformly transmitted to the loading beam on the top of specimen through the rigid bearing beam. The vertical load was slowly increased to the predetermined axial pressure by 2-3 times of loading and then was remained constant through the load regulating device. Subsequently, the horizontal cyclic load was applied. According to the JGJ 101-2015 Specification of Testing Methods for Earthquake Resistance Building, loading mechanism and load-displacement control were adopted. Before the specimen yielded, load control was utilized to exert load with an increment of 50 kN until yielding, and each grade of load underwent one circulation. The yielding load and the yielding displacement were determined by comprehensive observation of the loaded outermost longitudinal bars in the shear wall and the load-displacement curve when it obviously deviated from the

line. After the specimen yielded, displacement control was adopted to load. The load method was circularly exerted with a multiple of yield displacement  $\Delta_y$  and a three-time circulation for each grade of displacement, until the specimen was failure, unavailable loading, or the load decreasing to about 85% of the maximum load.

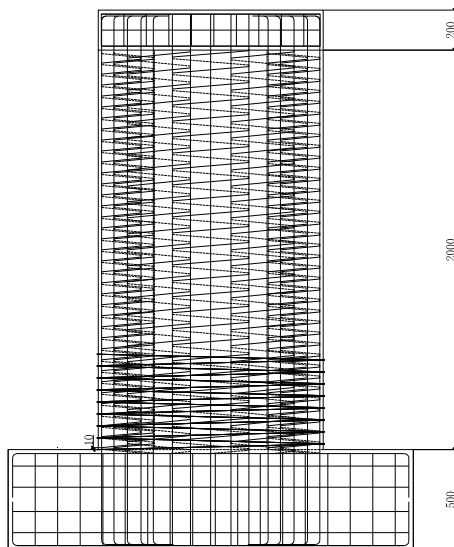
### 2.3 Test content and measuring-point arrangement

Major content of the test includes: (1) cyclic horizontal load and its corresponding displacement of each grade circulation at the horizontal loading point of the wall top; (2) bending deformation, shearing deformation, rebar sliding deformation, and the total horizontal displacement of the plastic hinge region; (3) rigid displacement of the grade beam; (4) strain of the longitudinal reinforcement steels in plastic hinge region of the wall, strain of stirrups, and strain of horizontally and vertically-distributed reinforcement bars; (5) load-displacement hysteresis loop of the specimen under recycling load.

Fig. 3 showed the arrangement of displacement meters.



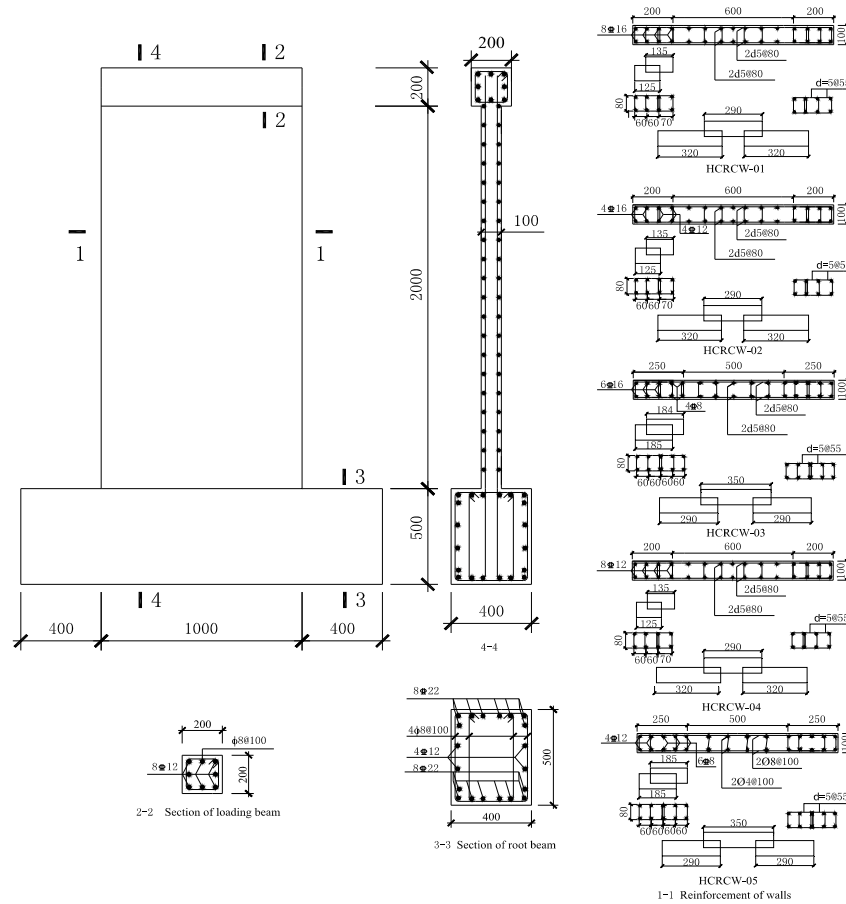
(a) HRSR in the shear wall



(b) Outer HRSR in the shear wall



Fig. 1 Structure and reinforcement of shear walls



(c) Dimensions of walls and arrangement of reinforcement

Fig. 1 Continued

Table 1 Parameters of specimens

Specimen number	The range of outer HRSR	$\lambda$	$n$	$\rho_s\%$	Stirrup in embedded column	$\rho_{sv}\%$	Reinforcement of wall	
							Horizontal reinforcement / ( $\rho_h\%$ )	Vertical reinforcement / ( $\rho_v\%$ )
HCRCW-01	None	2.1	0.22	8.0	d5@55	0.7	d5@80	d5@80
HCRCW-02	None	2.1	0.22	6.3	d5@55	0.7	d5@80	d5@80
HCRCW-03	480 mm high from bottom of the wall	2.1	0.22	5.6	d5@55	0.7	d5@80	d5@80
HCRCW-04	All of the wall	2.1	0.22	4.5	d5@55	0.7	d5@80	d5@80
HCRCW-05	None	2.1	0.17	3.0	d5@55	0.7	$\phi 8@100$	$\phi 4@100$
SW11	None	2.0	0.20	3.0	$\phi 6@80$	0.6	$\phi 6@125$	$\phi 6@125$

\*  $\lambda$ : shear span ratio;  $\rho_s$ : longitudinal reinforcement ratio of the embedded columns;  $\rho_{sv}$ : area stirrup ratio;  $\rho_h, \rho_v$ : horizontal distribution reinforcement ratio and vertical distribution reinforcement ratio of wall, respectively

Each specimen was assembled with ten displacement meters, among which six were YHD-1000L guyed displacement meters. Displacement meter A was horizontally assembled at the center of the loading beam on the wall top (2100 mm high from the wall bottom) in order to measure the horizontal displacement of the specimen apex. Displacement meter J was horizontally assembled the height of 1900 mm from the wall bottom, in order to measure the total horizontal displacement of this height range. Guyed displacement meters C and I were vertically

configured at the height of 1000 mm from the wall bottom to measure the bending deformation within the height range. Simultaneously, a horizontal displacement meter B was assembled at the same height to measure the total horizontal displacement of this height range. Guyed displacement meters G and H were assembled along the diagonal cross at the height of 1000 mm from the wall bottom for the measurement of shearing deformation in this region. At the height of 300 mm from the wall bottom, two gyyed displacement meters, E and F, were vertically

Table 2 Mechanical properties of reinforcement

Steel bar	Steel type	$f_y / \text{N} \cdot \text{mm}^{-2}$	$f_u / \text{N} \cdot \text{mm}^{-2}$	$A_s / \%$
High-strength steel bar	$d = 5$	965	1120	10
	$\Phi 8$	437.5	665	25
HRB400	$\Phi 12$	437.5	585	25
	$\Phi 16$	452.5	610	25

\*  $f_y, f_u$ : test average of steel yield strength and tensile strength, respectively;  $A_s$ : reinforced elongation

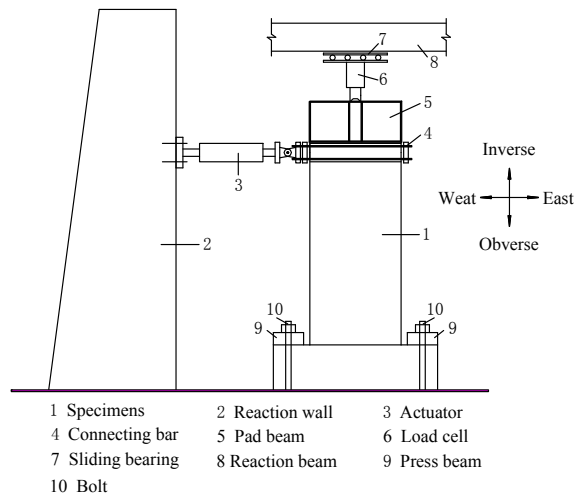
Table 3 Mechanical properties of concrete

Concrete grade	$f_{cu} / \text{MPa}$	$f_{cu,m} / \text{MPa}$	$f_{c,m} / \text{MPa}$
C50	65.91, 57.36, 60.42 / 50.69, 52.51, 55.70	57.1 MPa	37 MPa

\*  $f_{cu}$ : cube compressive strength measured value of the standard cube test block under the same condition for 28 days;  
 $f_{cu,m}$ : the average value measured of the cube compressive strength;  $f_{c,m}$ : the average value of the axial compressive strength



(a) Loading device



(b) Schematic diagram

Fig. 2 Test set-up

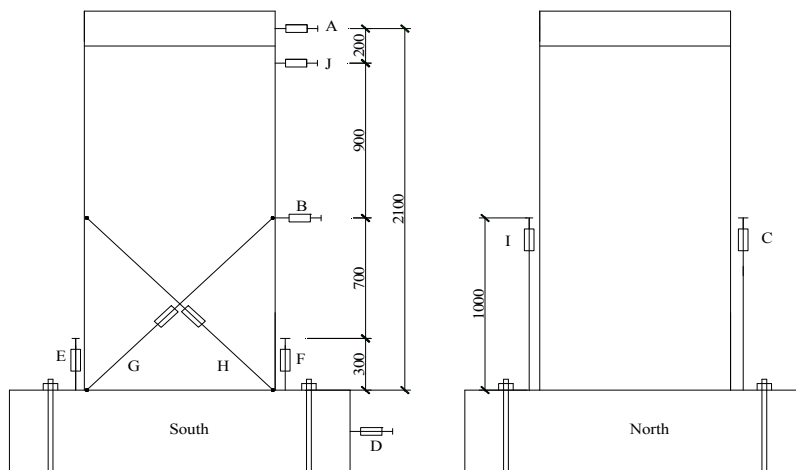


Fig. 3 Arrangement of the displacement measuring points

arranged to measure the bending deformation of the wall in the concentration area of plastic deformation. A horizontal

displacement meter D was assembled at the end of the mudsill to monitor the overall horizontal slipping of the specimen.

### 3. Results and discussion

#### 3.1 Test phenomenon

##### (1) Specimen of HCRCW-01

When the horizontal thrust reached 150 kN, apex displacement of the specimen was 2.3 mm (displacement angle  $\theta = 1/909$ ), and multiple tiny cracks occurred in the tensile region of the wall. When was increased to 250 kN, long and thin bending diagonal shear cracks appeared. Under the further loading till specimen yielding, there were multiple newly-added horizontal cracks at the lower part of the wall, and the original horizontal cracks unceasingly grew and extended. With the increase of the load, multiple horizontal cracks extended into bending shear diagonal cracks, and the scope of newly-added cracks was continuous upward, the number of cracks was increasing, the average spacing of crack was about 50 mm. When the horizontal load was increased to 350 kN, the longitudinal tensile reinforcement of the shear wall yielded, the apex displacement was approximately 8.6 mm ( $\theta = 1/244$ ). Then a remarkable deviation of load-displacement curve from the line was observed, it was indicative of the beginning of component yielding. At this very moment, the assumed yield displacement  $\Delta_y$  was represented by the corresponding displacement, loading turned to be controlled by displacement, and loading circulation was conducted according to a multiple of  $\Delta_y$  with three times of circulation in each grade of displacement. When it was recycled to the first lap of  $2\Delta_y$ , a lot of slender inclined cracks of about 60 degrees appeared in the upper part of the wall. The original cracks unceasingly extended and widened. Meanwhile, a vertical crack appeared near the outermost longitudinal bars in the compression zone of the wall bottom, the concrete protective layer in the compression region on the wall bottom began to crumble. When it was recycled to the first lap of  $3\Delta_y$ , the horizontal cracks at the bottom of the wall seriously widened, some of more obvious inclined cracks were formed in the wall body. When it was recycled to the third lap of  $3\Delta_y$ , blocks of the concrete protective layer in the compression region on the wall bottom falling off. When it was recycled to the first lap of  $4\Delta_y$ , the diagonal cracks and the horizontal cracks widened with a maximum width of 0.8 mm and 1.2 mm, respectively. Most concrete in the plastic hinge region on the wall bottom fell off. When it went to  $5\Delta_y$ , concrete on both sides of the wall bottom fell off and the dropping area continuously spread towards the center of the wall, forming a penetrating zone. The carrying capacity of specimen declined to below 85% of the maximum load, and the specimen suffered the flexural failure by compression. When specimen HCRCW-01 was damaged, fracture and buckling happened to the longitudinal bars and significant buckling happened to the vertical steel bars. Under the action of large vertical load, concrete in the plastic hinge region of the wall bottom was crushed on the whole cross section. Slight buckling occurred on horizontally-distributed reinforcement bars in the wall. However, the confining stirrups and horizontally-distributed steel were not broken during the damage. During the whole loading process, there was no obvious shear slip

deformation.

##### (2) Specimen of HCRCW-02 to HCRCW-04

Compared with specimen HCRCW-01, specimens HCRCW-02 to HCRCW-04 had small ratio of longitudinal reinforcement, similar failure pattern of each stage, but different failure properties. For HCRCW-02, the peak load was lower, the development of the inclined cracks in the wall was not sufficient, the distribution was relatively sparse, and the coverage of the inclined cracks was narrow.

Besides smaller ratio of longitudinal reinforcement, specimens HCRCW-03 and HCRCW-04 were equipped with outer HRSR with a diameter 5 mm spacing 60 mm in the plastic hinge region and wall body, respectively. During the loading process of HCRCW-03, horizontal cracks and inclined cracks developed fully, dense and uniform on the wall. When HCRCW-03 was damaged, the outer HRSR serious buckling, the spiral stirrups and horizontally-distributed steel were not broken during the damage. Compared to HCRCW-02, the load carrying capacity and displacement of specimen HCRCW-03 were higher. The reason was that the outer HRSR set in the bottom plastic hinge region, limited the falling off of concrete protective layer, delayed the occurrence of longitudinal reinforcement buckling and the occurrence of specimen failure.

Compared with HCRCW-03, the ratio of longitudinal reinforcement was smaller of HCRCW-04. They had the similar failure pattern of each stage. The differences were that when HCRCW-04 was damaged, the outer HRSR was slightly buckling, the core concrete at the bottom of wall locally was spall. Bending cracks were dominant in the crack distribution, and the failure modes of HCRCW-04 were flexural failure by compression. The peak load was lower, but the wall deformation was approximately the same with HCRCW-03. Cracks were mainly concentrated in the middle lower part of the wall, no cracks in the upper part. It was showed that outer HRSR could significantly improve the deformation of the wall, and control the crack in the lower range and restrict cracks to develop upward.

##### (3) Specimen of HCRCW-05

Specimen HCRCW-05 was a reference specimen. During the loading process, bond slip phenomenon occurred. When damaged, fracture and buckling happened to the longitudinal bars, the core concrete at the bottom of wall locally falling off, and the failure modes of HCRCW-05 was flexural failure by compression. Compared with SW11 in literature (Zhang *et al.* 2009), both of the specimens HCRCW-05 and SW11 occurred to flexural failure, and the parameters of embedded columns were basically consistent except for stirrup form, but the failure phenomenon were different. The horizontal cracks of HCRCW-05 were dense and uniform, high-strength spiral reinforcements at the bottom of the compression zone of the wall were not collapsed or fractured, which provided restraint of core concrete effectively. Finally, concrete in the compression zone only was locally spall.

Failure patterns and cracks of the five shear wall specimens were shown in Fig. 4.

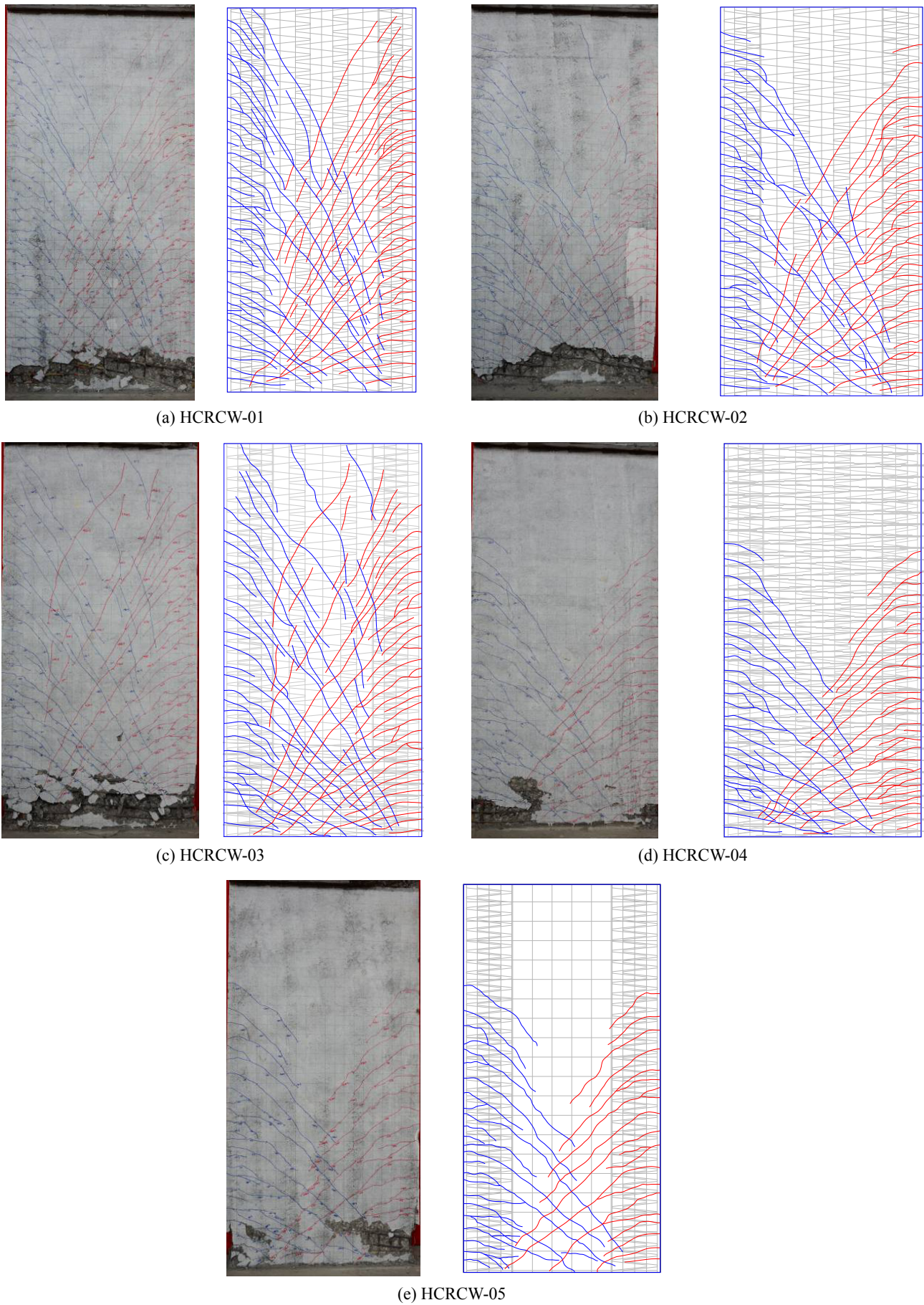


Fig. 4 Damage patterns and cracks distribution of specimens

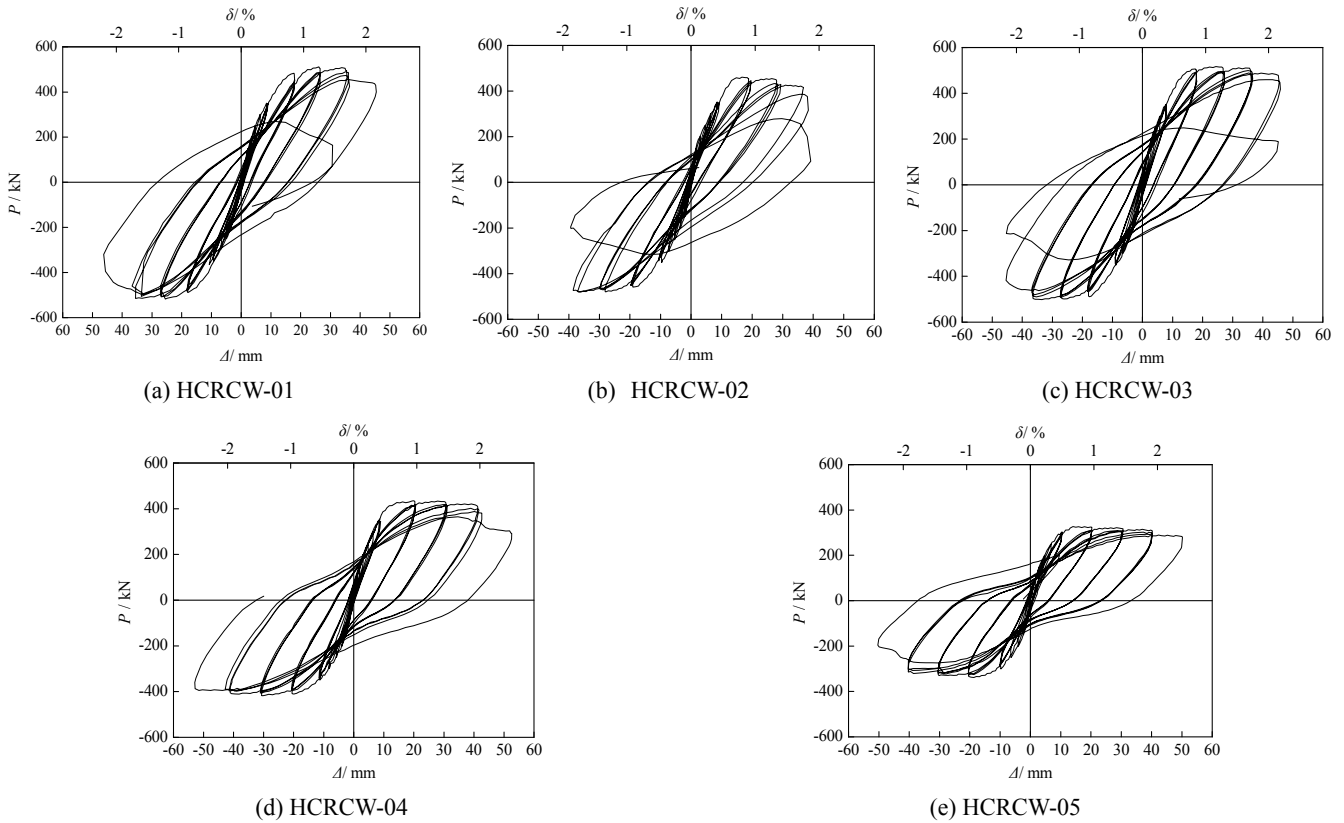


Fig. 5 Hysteretic curves of specimens

### 3.2 Hysteresis loop and skeleton curve

The load-displacement hysteresis loops and skeleton curves of the five shear walls manufactured were demonstrated in Figs. 5-6. Through comparison analysis of Fig. 5, it was known that these specimens shared the following common properties and laws. Before cracking, the specimen was essentially in the elastic stage and the loading and unloading curves were almost coincided into a line. From the time of specimen cracking to the moment before specimen yielding, the hysteretic curve only encircled a tiny area and the loop was narrow and spindly, indicating no significant variation of the overall stiffness.

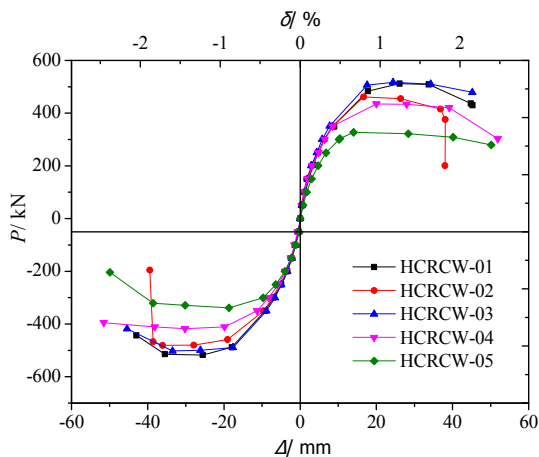


Fig. 6 Skeleton curve of specimens

Residual deformation and energy dissipation were quite low. After the tensile reinforcement bars yielded, the area encircled by the hysteresis loop gradually increased and the energy dissipation unceasingly climbed. Under the same grade of displacement control, load carrying capacity and stiffness in the latter two circulations were slightly lower than those in the first circulation.

When the peak load was reached, the specimens showed a certain degree of decline in the load carrying capacity, a decrease in stiffness, and a continuous increase in the hysteresis area, hysteresis loop were rather plump. It can be clearly observed from the hysteresis curve shown in Fig. 5, hysteresis loops of HCRCW-01 to HCRCW-03 were spindle shaped without the pinching phenomenon, and the walls exhibited fairly good deformability. Besides, hysteresis loop diagonal angle was larger, which indicated that the shear wall in the mutual nesting of high-strength spiral hoops enhanced the overall stiffness of the wall in a certain extent, and lead to reduce the shear slip. Skeleton curves of each specimen were shown in Fig. 6, from which it was seen that: Before specimens HCRCW-01 to HCRCW-04 yielded, their skeleton curves almost coincided, showing that their elastic stiffness were rather close. When the displacement angles were 1%, the specimens reached their peak loads. After the specimens reached peak load, all the skeleton curves displayed a significant decline.

For the specimens HCRCW-01 to HCRCW-04, the longitudinal reinforcement ratio was reduced in turn. It was seen from Figs. 5-6, the longitudinal reinforcement ratio of HCRCW-01 was larger, hysteresis loops were plump and

Table 4 Characteristic loads of specimens

Specimen Number	$P_{cr}$ / kN			$P_y$ / kN			$P_m$ / kN			$P_u$ / kN		
	Pos.*	Neg.	Ave.	Pos.	Neg.	Ave.	Pos.	Neg.	Ave.	Pos.	Neg.	Ave.
HCRCW-01	204.3	150.2	177.3	350.6	350.6	350.6	511.9	517.7	514.8	435.1	440.0	437.6
HCRCW-02	200.2	150.6	175.4	350.7	350.4	350.6	461.2	480.7	470.9	392.0	408.6	400.3
HCRCW-03	150.0	149.7	149.9	350.9	350.4	350.7	516.8	501.8	509.3	439.3	426.6	432.9
HCRCW-04	150.5	149.9	150.2	350.5	349.5	350.0	435.0	417.8	426.4	369.8	355.1	362.4
HCRCW-05	150.3	99.9	125.1	300.1	300.2	300.1	327.1	338.5	332.8	278.0	287.7	282.9

\* Pos.: positive, Neg.: negative, Ave.: average

Table 5 Characteristic displacement and ductility

Specimen Number	$\Delta_{cr}$			$\Delta_y$			$\Delta_m$			$\Delta_u$			ductility coefficient
	Pos.	Neg.	Ave.	Pos.	Neg.	Ave.	Pos.	Neg.	Ave.	Pos.	Neg.	Ave.	
HCRCW-01	3.5	2.3	2.9	8.6	9.2	8.9	26.1	25.5	25.8	44.9	43.3	44.1	5.0
HCRCW-02	3.0	2.1	2.6	8.4	9.6	9.0	16.7	36.1	26.4	35.8	36.9	36.3	4.0
HCRCW-03	2.0	2.2	2.1	7.8	8.8	8.3	24.4	33.5	28.9	45.2	44.2	44.7	5.4
HCRCW-04	2.0	2.4	2.2	8.5	—	8.5	20.0	30.2	25.1	44.8	—	44.8	5.3
HCRCW-05	3.0	1.1	2.1	10.2	9.7	10.0	14.0	18.7	16.3	50.6	41.8	46.2	4.6

Table 6 Comparison of characteristic parameter

Specimen Number	$P_y/P_{cr}$	$P_m/P_y$	$\Delta_y / \Delta_{cr}$	$\Delta_m / \Delta_y$	$\theta = \frac{\Delta_u}{H}$
HCRCW-01	2.42	1.20	4.77	1.88	1/48
HCRCW-02	2.22	1.21	4.77	2.16	1/58
HCRCW-03	2.81	1.21	6.18	2.26	1/47
HCRCW-04	2.40	1.18	3.8	3.00	1/47
HCRCW-05	2.26	1.18	4.22	1.87	1/46

recycle numbers were more. Compared with other specimens, the loads in the each stage of HCRCW-01 were significantly improved, descent segment of skeleton curve declined smoothly. The longitudinal reinforcement ratio of HCRCW-02 was smaller than HCRCW-01, and the load carrying capacity of the wall decreased. In the later stage of loading, the tensile longitudinal bars were broken, the load carrying capacity of the specimen was deteriorated rapidly, and the skeleton curve decreased steeply.

Longitudinal reinforcement ratio of specimens HCRCW-03 and HCRCW-04 decreased contrast to HCRCW-02, but load carrying capacity had improved significantly. That was because outer HRSR were set in the bottom plastic hinge region and wall body of HCRCW-03 and HCRCW-04, respectively. It can effectively restrain the concrete protective layer, control the falling off of the concrete, delay the occurrence of longitudinal reinforcement buckling and the occurrence of specimen failure.

Figs. 5-6 showed that the specimens HCRCW-03 and HCRCW-04 presented a more plump hysteretic behavior; the two specimens had almost no decrease in the load carrying capacity and without rapid stiffness deterioration after the peak load. However, the pinching phenomenon existed obviously on the hysteresis curve of HCRCW-04,

yet it was not found on HCRCW-03. The major difference between HCRCW-03 and HCRCW-04 was longitudinal reinforcement ratio of the embedded columns, so the longitudinal reinforcement ratio was a more important parameter to pinching behavior.

From Fig. 5 it can be observed that the pinching shrinkage phenomenon of HCRCW-05 was more obvious and hysteretic curve was inclined to the horizontal axis, indicating that the stiffness was weak. The reason was that the wall body with ordinary form of horizontal distribution reinforcement of the wall, which cannot form an effective constraint, led to a weak stiffness of the wall.

Contrast to SW11 of literature (Zhang *et al.* 2009), HCRCW-05 had a stronger bearing load, nearly 27% growth compared to SW11, indicating that the embedded columns of wall confined with high-strength spiral stirrups improved the compressive strength of core concrete and the ultimate deformation capacity, effectively promoted the shear wall load carrying capacity.

### 3.3 Deformability and energy dissipation

#### 3.3.1 Deformability

The cracking load and corresponding displacement were

determined by tiny cracks appearing on the wall. Based on the strain of longitudinal bar in the embedded columns reached the yield strain, the yield load and corresponding displacement were determined using the equivalent energy method. The maximum load and its displacement in the skeleton curve were regarded as the peak load and the corresponding displacement. The load at the moment of declining to 85% of the peak was regarded as the failure load, the corresponding displacement as the ultimate displacement. Displacement ductility was determined according to the ratio of the ultimate displacement to the yield displacement. The load and displacement of characteristic points of each specimen were shown in Tables 4-5.

It can be seen from Tables 5-6, the ductility coefficients of HCRCW-01 to HCRCW-04 were above 4.0, which indicated that deformation of the high-strength concrete shear wall was good when confined with HRSR. From the ductility coefficient and story drift were shown in Tables 5-6, deformation capacity of HCRCW-03 and HCRCW-04 was better than HCRCW-01 and HCRCW-02. Contrast HCRCW-03 and HCRCW-04 to HCRCW-02, ductility coefficients increased by 33% and 35%, respectively. It

indicated that when the axial-compression ratio was the same, deformation capacity of the wall outer HRSR in the plastic hinge region or wall was significantly improved. Compared with HCRCW-02, ductility coefficient of specimen HCRCW-01 increased by 25%. It stated clearly that dense longitudinal reinforcement and closed spiral stirrups effectively constrained the internal core concrete to ensure integrity of columns and kept bearing capacity, so as to give full play to the role of the embedded columns, provide a good end restraint for the entire wall. At the same time, high-strength spiral horizontal distribution reinforcements provided higher shear capacity for the wall, thus making the design concept of “strong shear weak bending” was easily guaranteed, as well as the plastic deformation ability of high-strength concrete shear wall had been enhanced.

HRSR was only adopted in the embedded columns of HCRCW-05, its ductility coefficient was 4.6, and the layer drift angle was 1/46. The ductility coefficient of specimen SW11 (Zhang *et al.* 2009) was 2.81, and the layer drift angle was 1/116. Compared with the SW11, the deformation ability of HCRCW-05 was up 63%.

Table 6 showed that, values of  $P_y/P_{cr}$  of specimens HCRCW-01 to HCRCW-05 were within 2.2-2.81, indicating that the specimen load carrying capacity experienced substantial increase from the cracking to the yielding stages. The  $P_m/P_y$  value within 1.18-1.21 showed that during the period from the yielding to the peak load, the specimen load carrying capacity increased slightly. Values of  $\Delta_y/\Delta_{cr}$ ,  $\Delta_m/\Delta_y$ , and story drift ratio  $\theta$  were in the ranges of 4.22-6.18, 1.87-2.36, and 1/58-1/46, respectively, which showed the specimen deformability enhanced during the process from cracking to yielding then to failure. It satisfied the specification requirement of elastic-plastic story drift angle limit  $\theta_p = 1/120$  of the shear wall structure.

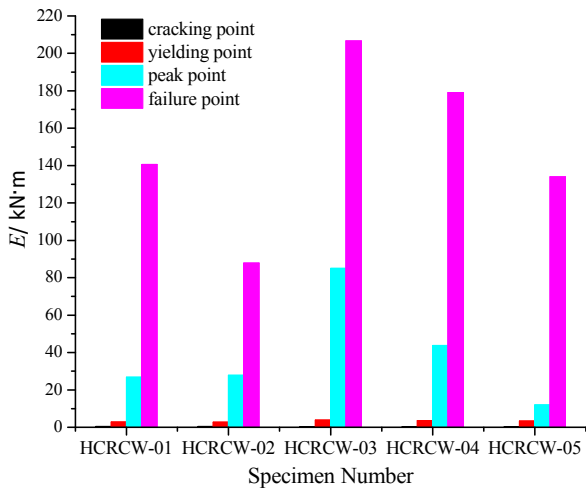
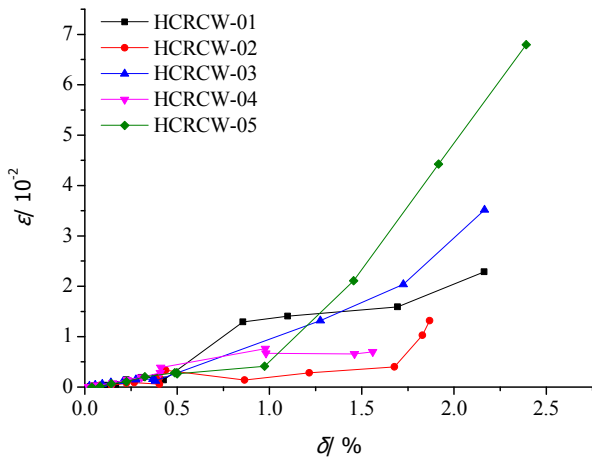


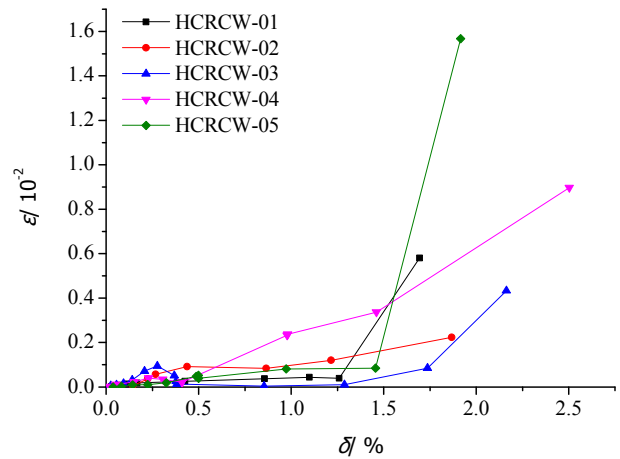
Fig. 7 Energy dissipations of specimens

### 3.3.2 Energy dissipation

Energy dissipation reflected the energy absorbing capacity of the element in the cyclic loading process. It was a critical index to measure the seismic ability, which used the area encircled by the load-displacement hysteresis loop in the measurement. Generally, the larger the area encircled



(a) Compression strain of column



(b) Compression strain of wall

Fig. 8 Compressive strain of column and wall at different displacement

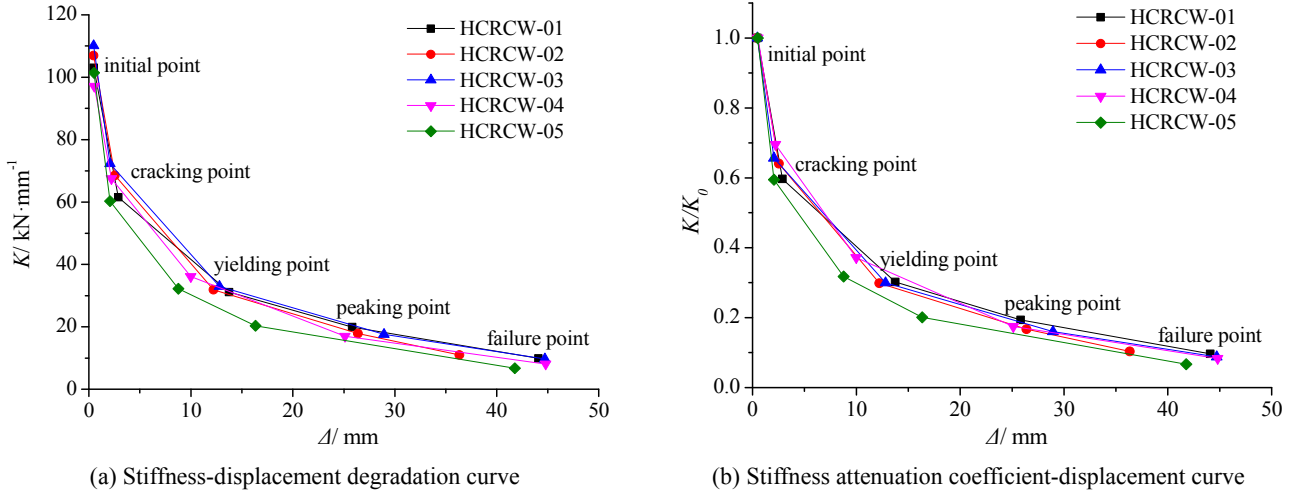


Fig. 9 Stiffness degradation curves of specimens

by the hysteresis loop, the plumper the curve, the more the dissipated energy by the specimen, and the stronger the energy dissipation capability.

Fig. 7 exhibited the accumulated energy dissipation of specimens HCRCW-01 to HCRCW-05 at the cracking, yielding, peak, and failure points. It was seen from Fig. 7, Energy dissipation capacity of HCRCW-03 and HCRCW-04 was better than HCRCW-01 and HCRCW-02. It indicated that when longitudinal reinforcement ratio was suitable, outer HRSR set in plastic hinge regions or wall body with internal steel reinforcement framework together formed dual constraints on the core concrete, showed strong energy dissipation capacity; Compared specimen HCRCW-05 with SW11 in literature (Zhang *et al.* 2007), the energy dissipation capacity was doubled compared with SW11.

It was obviously observed from Fig. 7 that during the process from the peak point to the ultimate point, specimen capacity of energy dissipation was significantly improved. It proved that specimens adopting the high-strength spiral stirrup and the high-strength spiral horizontally distributed reinforcements all had superior capacity of energy dissipation after the peak load. The reason was that after the peak load, high-strength spiral stirrups in embedded columns sufficiently played the role of confinement and delayed the concrete crushing and longitudinal bar yielding. The high-strength spiral horizontally distributed bars in the wall well confined the concrete to prevent the untimely crushing of concrete on the wall bottom, making concrete perform a good ductility.

### 3.4 Compressive strain

Fig. 8 showed the axial strain of the embedded columns and the wall near the embedded columns zone after the specimen was damaged by cyclic loading, where  $\delta$  stood for the wall displacement angle.

It was seen from the Fig. 8: compression strain of column and wall increased with the increase of displacement, but the growth rate was different. The longitudinal reinforcement ratio of HCRCW-01 was larger, compression strain increased slowly. Compared with HCRCW-01, the longitudinal reinforcement ratio of HCRCW-02 was

smaller, compression strain of column increased rapidly.

Longitudinal reinforcement ratio of specimen HCRCW-03 and specimen HCRCW-04 was small, but the strain grew slowly. It indicated that outer HRSR in the plastic hinge region or wall significantly constrained core concrete, improved the compressive strength of concrete, prevented the longitudinal deformation of concrete and buckling of longitudinal bars.

The axial-compression ratio of HCRCW-05 was small, Fig. 8(b) showed that compressive strain of the embedded column and wall had a rapid increase when the displacement angle reached around 1.0% and 1.5%, respectively. That's due to small longitudinal reinforcement ratio and inferior constrain of wall. When the longitudinal reinforcement ratio was smaller, the axial compression strain of embedded column increased with the increase of horizontal displacement. High axial compressive stress of embedded column drove the column to fail and transmitted the extra axial pressure to the wall. The sudden increase of the axial stress accelerated the wall damage, making the wall show a poor deformability.

### 3.5 Stiffness deterioration

The secant stiffness was used to express stiffness of specimen at all levels of load, the secant stiffness  $K_i$  which was calculated by Eq. (1). The  $i^{\text{th}}$  secant of the specimen was equal to the ratio of the sum of absolute values of positive and negative peak loads in the  $i^{\text{th}}$  circulation to the sum of absolute values of the corresponding displacements.

$$K_i = \frac{|+P_i| + |-P_i|}{|+\Delta_i| + |-\Delta_i|} \quad (1)$$

where  $P_i$  was the peak load of the  $i^{\text{th}}$  circulation and  $\Delta_i$  was the peak point displacement of the  $i^{\text{th}}$  circulation.

The stiffness deterioration curves of the specimens were shown in Fig. 9. As shown in Fig. 9(a), under the action of cyclic horizontal load, with the increase of load and displacement amplitude, the plastic deformation unceasingly increased and specimen stiffness gradually deteriorated. For the convenience of comparison, the

displacement-relative stiffness curve was plotted as shown in Fig. 9(b). Relative stiffness was defined as the ratio of measured stiffness of each specimen to the initial stiffness during the test. It can be observed that the stiffness deterioration trends of each specimen were roughly the same. In the period from initial loading to specimen cracking, the stiffness deteriorated most rapidly to only 60% of the initial stiffness. In the process from specimen cracking to yielding, the stiffness deteriorated less rapidly. Most cracks of the specimens occurred in this stage. After the specimens yielded, the stiffness deteriorated slowly with on a few newly-added cracks. This was identical with the specimen stiffness deterioration curves.

Fig. 9 presented that before peak load and under the same axial-compression ratio, the larger the longitudinal reinforcement ratio, the smoother the stiffness deterioration. The deformation capacity of the wall was effectively promoted when outer HRSR was arranged in the plastic hinge region or the wall, and stiffness degenerated slowly. Under different axial-compression ratios, the stiffness deterioration receded with the increase of axial-compression ratio. After reaching the peak load, the stiffness degradation trend gradually decreased, and the stiffness degradation curve of each specimen was basically the same.

#### 4. Conclusions

RC shear walls confined with HRSR were proposed in this paper. Their seismic performances were experimentally studied. Pseudo static tests were performed on five RC shear walls confined with HRSR possessing different parameters. The following conclusions can be drawn:

- The restraint pattern of the shear walls confined with HRSR limited the lateral expansion of concrete, increased ultimate compressive stress of core concrete. That showed significant capability of axial compressive strength and deformation without a rapid deterioration of axial strength after reaching the peak load.
- Outer HRSR set in the plastic hinge region or the wall can effectively restrain the concrete protective layer. It was an available method of using the outer HRSR in plastic hinge region to enhance the seismic performance of shear walls, be similar to steel plate shear walls but with much less reinforcement, especially under the high axial-compression ratio.
- The pinching phenomenon of hysteresis curve was eliminated with the increase of the longitudinal reinforcement ratio.
- Test results showed that vertical distribution reinforcement with an exceedingly small diameter led to reinforcement buckling under the action of high vertical load, and further caused the horizontally-distributed reinforcement buckling. It can be observed from the vertical reinforcement strain that, most of the vertical steel bars did not yield. Therefore, large-diameter, low-strength reinforcement bars were suggested to be adopted.
- Because of the convenient and fast installation, the

shear walls confined with HRSR that can reduce the labor cost. At the same time, the higher strength and smaller diameter reinforcements can save lots of reinforcements, making energy-saving and emission-reduction.

#### Acknowledgments

The research is financially supported by the foundation of Xi'an University of Architecture and Technology (Grant No. QN1635) and is greatly appreciated. Special thanks go to Professor Weishan Jiang and Xinghu Zhang for their assistance in the testing at the Xi'an University of Architecture and Technology in preparing and construction of the specimens.

#### References

- Chen, Z.Y. (1997), "Development and utilization of high-strength and high-performance concrete", *China Civil Eng. J.*, **30**(5), 3-11.
- Chris, G.K. (2015), "Mechanics of external RC beam-column joints with rectangular spiral shear reinforcement: Experimental verification", *J. Exp. Solid Mech.*, **50**(6), 311-322.
- Chris, G.K. and Constantin, E.C. (2013), "Shear tests of reinforced concrete beams with continuous rectangular spiral reinforcement", *J. Constr. Build Mater.*, **46**(4), 86-97.
- Constantin, E.C., Chris, G.K., Chalioris, C.E., Karayannis, C.G. (2013), "Experimental investigation of RC beams with rectangular spiral reinforcement in torsion", *J. Eng. Struct.*, **56**(5), 286-297.
- De Corte, W. and Boel, V. (2013), "Effectiveness of spirally shaped stirrups in reinforced concrete beams", *J. Eng. Struct.*, **52**(3), 667-675.
- Eom, T.S., Kang, S.M., Park, H.G., Choi, T.W. and Jin, J.M. (2014), "Cyclic loading test for reinforced concrete columns with continuous rectangular and polygonal hoops", *J. Eng. Struct.*, **67**(2), 39-49.
- GB50011-2010 (2010), Code for seismic design of buildings; China Architecture & Building Press, Beijing, China.
- Jiang, H.T., Li, Q.N., Jiang, W.S. and Zhang, D.Y. (2016), "Study on seismic performance of connection joint between prefabricated prestressed concrete beams and high strength reinforcement-confined concrete columns", *Steel Compos. Struct., Int. J.*, **21**(2), 343-356.
- Jing, D.H., Yu, T. and Liu, X.D. (2016), "New configuration of transverse reinforcement for improved seismic resistance of rectangular RC columns: Concept and axial compressive behavior", *J. Eng. Struct.*, **111**, 383-393.
- Jonathan, W., Ahmed, I. and Riyadh, H. (2016), "Analytical compressive stress-strain model for high-strength concrete confined with cross-spirals", *J. Eng. Struct.*, **113**(1), 362-370.
- Liang, X.W., Deng, M.K., Zhang, X.H. and Tian, S. (2007), "Experimental study on performance-based seismic design of high performance concrete shear wall", *J. Build. Struct.*, **28**(5), 80-88.
- Liang, C.Y., Chen, C.C., Weng, C.C., Yin, S.Y.L. and Wang, J.C. (2014), "Axial compressive behavior of square composite columns confined by multiple spirals", *J. Constr. Steel Res.*, **103**(10), 230-240.
- Lonnie, M., Natalie, D., Will, L. and Riyadh, H. (2014), "Axial behavior of high-strength concrete confined with multiple spirals", *J. Eng. Struct.*, **60**(1), 68-80.
- Karayannis, C.G. and Sirkelis, G.M. (2005), "Response of

- columns and joints with spiral shear reinforcement”, *WIT Trans. Modell. Simul.*, **41**, 455-463.
- Karayannis, C., Sirkelis, G. and Mavroeidis, P. (2005), “Improvement of seismic capacity of external beam-column joints using rectangular spiral shear reinforcement”, *WIT Transactions on The Built Environment*, **81**.
- Tsonos, A.G. (2004), “Improvement of the earthquake resistance of R/C beam-column joints under the influence of  $P - \Delta$  effect and axial force variations using inclined bars”, *J. Struct. Eng. Mech.*, **18**(4), 389-410.
- Tsonos, A.G. (2007), “Cyclic load behavior of RC beam-column sub-assemblages of modern structures”, *J. ACI Struct.*, **104**(4), 468-478.
- Yin, S.Y.L, Wang, J.C. and Wang, P.H. (2012), “Development of multi spiral confinements in rectangular columns for construction automation”, *J. China Inst. Eng.*, **35**(3), 309-320.
- Zhang, H.M. (2007), “Study on the performance-based seismic design method for shear wall structures”, Ph.D. Dissertation; Tongji University, Shanghai, China.
- Zhang, S., Lv, X.L. and Zhang, H.M. (2009), “Experimental and analytical studies on the ultimate displacement of RC shear walls”, *China Civil Eng. J.*, **42**(4), 10-16.